J Solid State Electrochem (2012) 16:2631–2638
DOI 10.1007/s10008-012-1661-3

ORIGINAL PAPER

Nanostructured cobalt oxide-based composites for rechargeable Li-ion batteries

Byeong-Chul Yu · Jae-O Lee · Jun Ho Song · Cheol-Min Park · Churl Kyoung Lee · Hun-Joon Sohn

Received: 2 December 2011 / Revised: 11 January 2012 / Accepted: 14 January 2012 / Published online: 25 February 2012
© Springer-Verlag 2012

Abstract Cobalt oxide-based nanocomposites are prepared using Co_3O_4, various metals (Al, Mg), carbon powders, and a simple high-energy mechanical milling technique. X-ray diffraction, X-ray photoelectron spectroscopy, and high-resolution transmission electron microscopy show that the cobalt oxide-based composites are mainly composed of nanostructured CoO/Al_2O_3, CoO/MgO, and Co_3O_4/C composites, respectively. Based on concepts related to the enhanced electrical conductivity of the Co_3O_4/C nanocomposite using conducting carbon matrix and to the resistance of inactive ceramic matrices (Al_2O_3, MgO) against active CoO particle growth during cycling, various nanostructured cobalt oxide-based composites are tested for use as anode materials. Among the composites, the Co_3O_4/C nanocomposite anode exhibits good electrochemical characteristics, such as high-capacity, good initial Coulombic efficiency, and long cycle behavior for Li-ion batteries.

Keywords Lithium secondary batteries · Electrode materials · Nanostructured composite · Cobalt oxide-based composites

B.-C. Yu · H.-J. Sohn
Department of Materials Science and Engineering,
Seoul National University,
Seoul 151-742, Republic of Korea

J.-O. Lee · C.-M. Park (✉) · C. K. Lee (✉)
School of Advanced Materials and System Engineering,
Kumoh National Institute of Technology,
Gumi, Gyeongbuk 730-701, Republic of Korea
e-mail: cmpark@kumoh.ac.kr
e-mail: cklee@kumoh.ac.kr

J. H. Song
Advanced Batteries Research Center,
Korea Electronics Technology Institute,
Seongnam, Gyeonggi 463-816, Republic of Korea

Introduction

Currently, graphite (LiC_6, 372 mAh g^{-1}; about 840 mAh cm^{-3}) is used as an anode material in rechargeable Li-ion batteries. However, higher-capacity alternatives have been actively researched, particularly for anode materials. Among the many possible alternatives [1–3], nanostructured transition-metal-based oxides have been the focused upon in a large number of studies because they show high capacity and rapid-rate capability [4–8]. Although transition-metal-based oxide systems have a high-energy density and rapid-rate capability, they suffer from low initial Coulombic efficiency and poor cycling behavior because of partially irreversible Li_2O phases and large volume changes during discharge/charge.

Among the many transition-metal-based oxide systems, Co_3O_4 has been studied widely as an anode material in Li-ion batteries [9–17]. Although, Co_3O_4 is generally considered to be a high-capacity material for Li-ion batteries, it shows a very low initial Coulombic efficiency and poor electrochemical reversibility between micron-sized Co_3O_4 and Li [4, 9–17].

Recently, nanostructured composite materials prepared by various synthetic tools have been considered as candidates for the anode material in lithium secondary batteries [18–21]. This is because the nanostructured composite materials offer the following advantages: (1) a high capacity due to their ability to provide a higher interfacial area, (2) a high rate capability by increasing the lithium ion diffusion rate, and (3) stable cycling behavior by accommodating the strain generated during the cycling (this is possible due to their superplasticity and high ductility) [22].

Among the many methods for preparing nanocomposite materials, the high-energy mechanical milling (HEMM) method is quite interesting because it provides well-dispersed nanocomposites composed of active and inactive nanocrystallites [23, 24].

In this study, new nanostructured composites, such as Co_3O_4/C, CoO/Al_2O_3, and CoO/MgO, were prepared by the simple HEMM technique. Among the composites, Co_3O_4/C nanocomposite was prepared by HEMM to compensate the poor electrical conductivity of Co_3O_4. The CoO/Al_2O_3 and CoO/MgO were synthesized by mechanochemical reduction using Co_3O_4 and Al (or Mg) via the following reactions:

$$3Co_3O_4 + 2Al \rightarrow 9CoO + Al_2O_3 (\Delta G^o = -1125.352 \text{ kJ mol}^{-1}, 298 \text{ K}) \quad (1)$$

$$Co_3O_4 + Mg \rightarrow 3CoO + MgO (\Delta G^o = -417.045 \text{ kJ mol}^{-1}, 298 \text{ K}) \quad (2)$$

where ΔG^o is the standard free energy.

Based on concepts related to the enhanced electrical conductivity of the Co_3O_4/C nanocomposite using conducting carbon matrix and to the resistance of inactive ceramic matrices (Al_2O_3, MgO) against active CoO particle growth during cycling, various nanostructured cobalt oxide-based composites were tested for use as anode materials with the aim of enhancing the electrochemical performance of the cobalt oxide anode in Li rechargeable batteries.

Experimental

The CoO/Al_2O_3 composite sample was synthesized using the following process. Stoichiometric amounts of Co_3O_4 (Aldrich, >99.9%, 10 μm), Al (Aldrich, 99.9%, −325 mesh), and stainless steel balls (diameters, 3/8 and 3/16 in.) were placed in a hardened steel vial with a capacity of 80 cm^3 and a ball-to-powder ratio of 20:1. For the full mechanochemical reduction given in Eq. 1, the molar ratio of Co_3O_4 to the Al powders used here was 3:2. The HEMM process (Spex-8000) was carried out under an Ar atmosphere for 6 h. The CoO/MgO composite sample was synthesized using Co_3O_4 and Mg (Daejung, 99%, −325 mesh) powders by following the procedure mentioned above. For the full mechanochemical reduction given in Eq. 2, the molar ratio of Co_3O_4 to the Mg powders used here was 1:1. The Co_3O_4/C composite sample was prepared using Co_3O_4 and amorphous carbon (Timcal, Super P) powders by following the procedure given above. Preliminary studies showed that Co_3O_4 and C were 80% and 20% by weight, respectively.

The various composite samples were characterized by X-ray diffraction (XRD, Rigaku, D-MAX 2500-PC), X-ray photoelectron spectroscopy (XPS, Kratos, AXIS), high-resolution transmission electron microscopy (HRTEM, FEI F20, operating at 200 kV), and HRTEM energy dispersive spectroscopy (HRTEM-EDS) (FEI F20). For the TEM observation, a dilute suspension was dropped on a C- or SiO-coated TEM grid and dried. Ex situ XRD was used to observe the structural changes occurring in the active materials during cycling. The electrodes were detached from the coin-type electrochemical cell, washed with diethyl carbonate (DEC), dried for 3 h in an Ar-filled glove box, and coated with Kapton tape, which served as a protective film.

For the electrochemical evaluation of the cobalt oxide-based nanocomposite test electrodes consisting of the active powder material (70 wt.%), carbon black (Denka black, 15 wt.%) was used as the conductor and polyvinylidene fluoride (PVDF) dissolved in *N*-methyl pyrrolidinone (NMP) was used as the binder (15 wt.%). Each component was mixed well to form a slurry, which was then coated on a copper foil substrate; the coating was followed by pressing and drying at 120 °C for 4 h under a vacuum. Laboratory-made coin-type electrochemical cells were assembled in an Ar-filled glove box using Celgard 2400 as the separator, Li foil as the counter and reference electrodes, and 1 M $LiPF_6$ in ethylene carbonate (EC)/DEC (1:1 by volume, Panax Starlyte) as the electrolyte. All the cells were tested galvanostatically between 0.0 and 3.0 V (vs. Li/Li^+) at a current density of 100 mA g^{-1} using a Maccor automated tester. Li was inserted into the electrode during the discharge step and extracted from the working electrode during the charge step.

Results and discussion

Figure 1a–d shows the XRD patterns of the Co_3O_4, Co_3O_4/C, CoO/Al_2O_3, and CoO/MgO composites, respectively. In Fig. 1b, all the peaks correspond to the Co_3O_4 phase with reduced crystallinity because of the HEMM process. The average Co_3O_4 crystallite size in the Co_3O_4/C composite as estimated using Scherrer's equation was approximately 17.2 nm. The XRD peaks in Figs. 1c and d show only CoO phases containing an amorphous phase and an exiguously developed MgO phase, respectively, with lower crystallinity than the Co_3O_4/C composite. The average CoO nanocrystallite size in the CoO/Al_2O_3 and CoO/MgO composites estimated using Scherrer's equation was approximately 7.2 and 11.3 nm, respectively. The presence of CoO phases indicated that the mechanochemical reduction reactions in Eqs. 1 and 2 proceeded well.

To investigate the amorphous phases in Fig. 1c and d, XPS analyses were conducted; Al_2O_3 (O; 1 s, 531.5 eV) and MgO (O; 1 s, 532.1 eV) phases were clearly detected, as shown in Fig. 2a and b, respectively. On the basis of the previous XRD and XPS analyses, the CoO/Al_2O_3 and CoO/MgO nanocomposites were confirmed to be composed of reduced nanocrystalline CoO phases with Al_2O_3 and MgO phases, respectively.

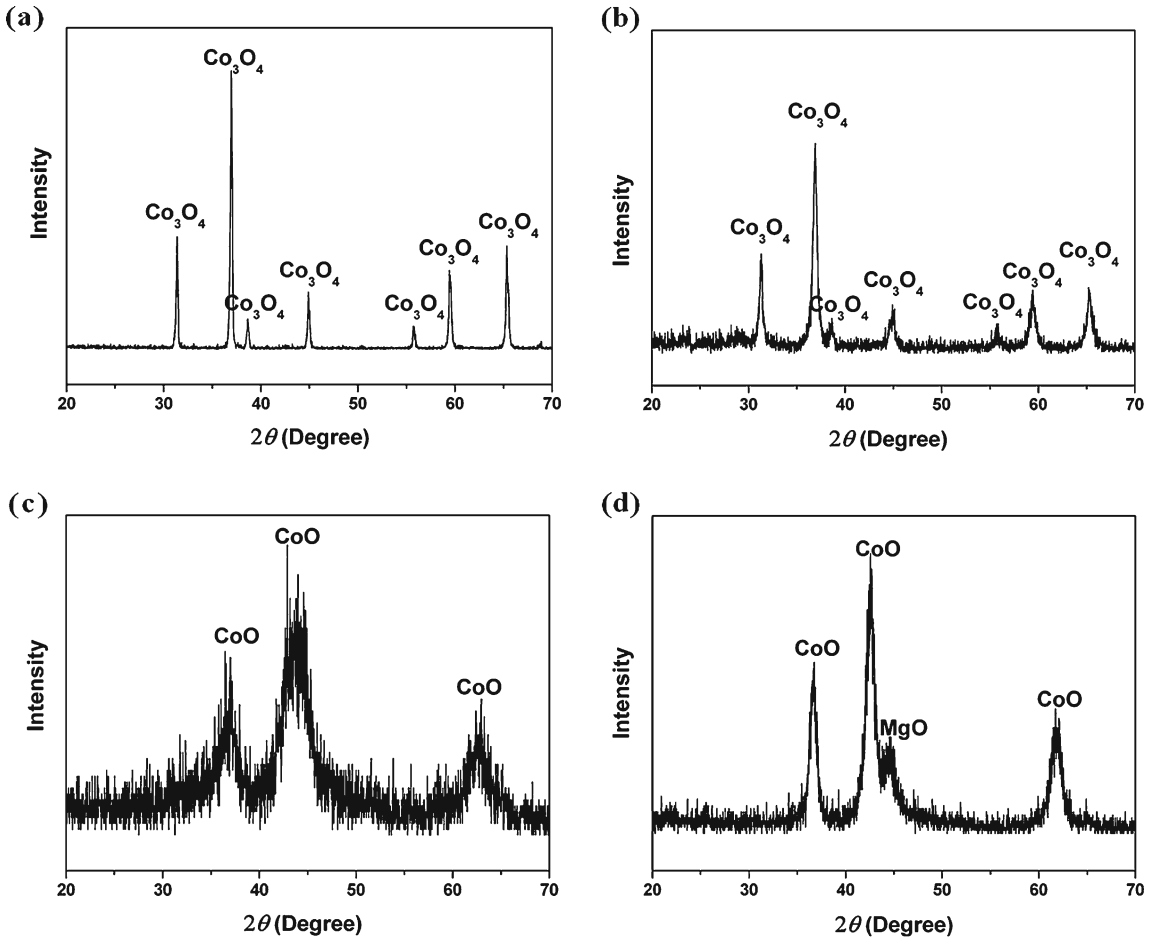

Fig. 1 Characterization of the cobalt oxide-based nanocomposites: **a** XRD pattern of Co_3O_4, **b** XRD pattern of Co_3O_4/C, **c** XRD pattern of CoO/Al_2O_3, **d** XRD pattern of CoO/MgO

HRTEM images along with selected-area diffraction (SAD) patterns and EDS mapping images showed the crystalline nanostructures of various cobalt oxide-based nanocomposites (Fig. 3). In Fig. 3a, the HRTEM image along with the SAD pattern and EDS mapping images shows the uniform dispersion of approximately 10–20 nm Co_3O_4 nanocrystallites in the amorphous carbon matrix, which agrees with that observed in the XRD pattern. Similarly, in Fig. 3b, the CoO/Al_2O_3 nanocomposite shows well-dispersed, approximately 5–15 nm CoO nanocrystallites

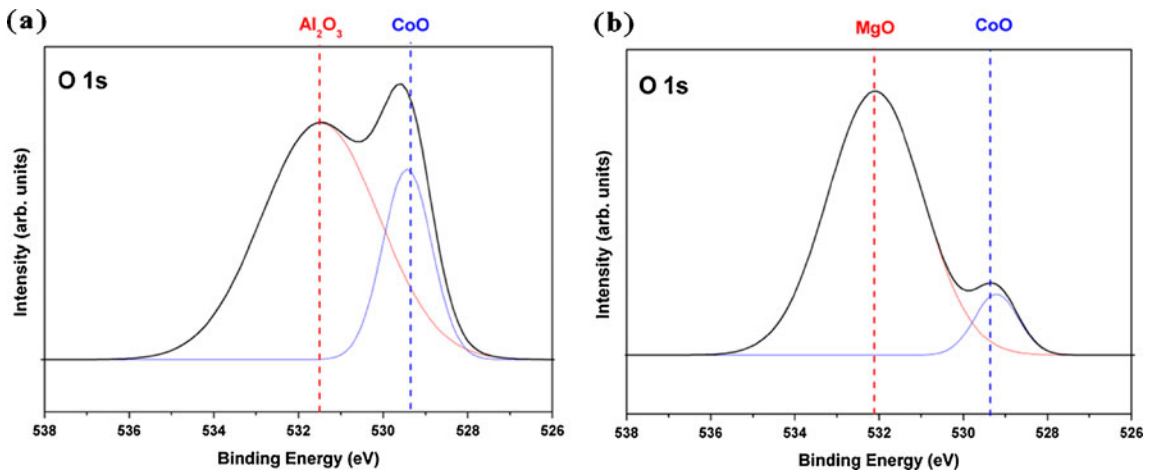

Fig. 2 XPS results of the cobalt oxide-based nanocomposites: **a** CoO/Al_2O_3 and **b** CoO/MgO

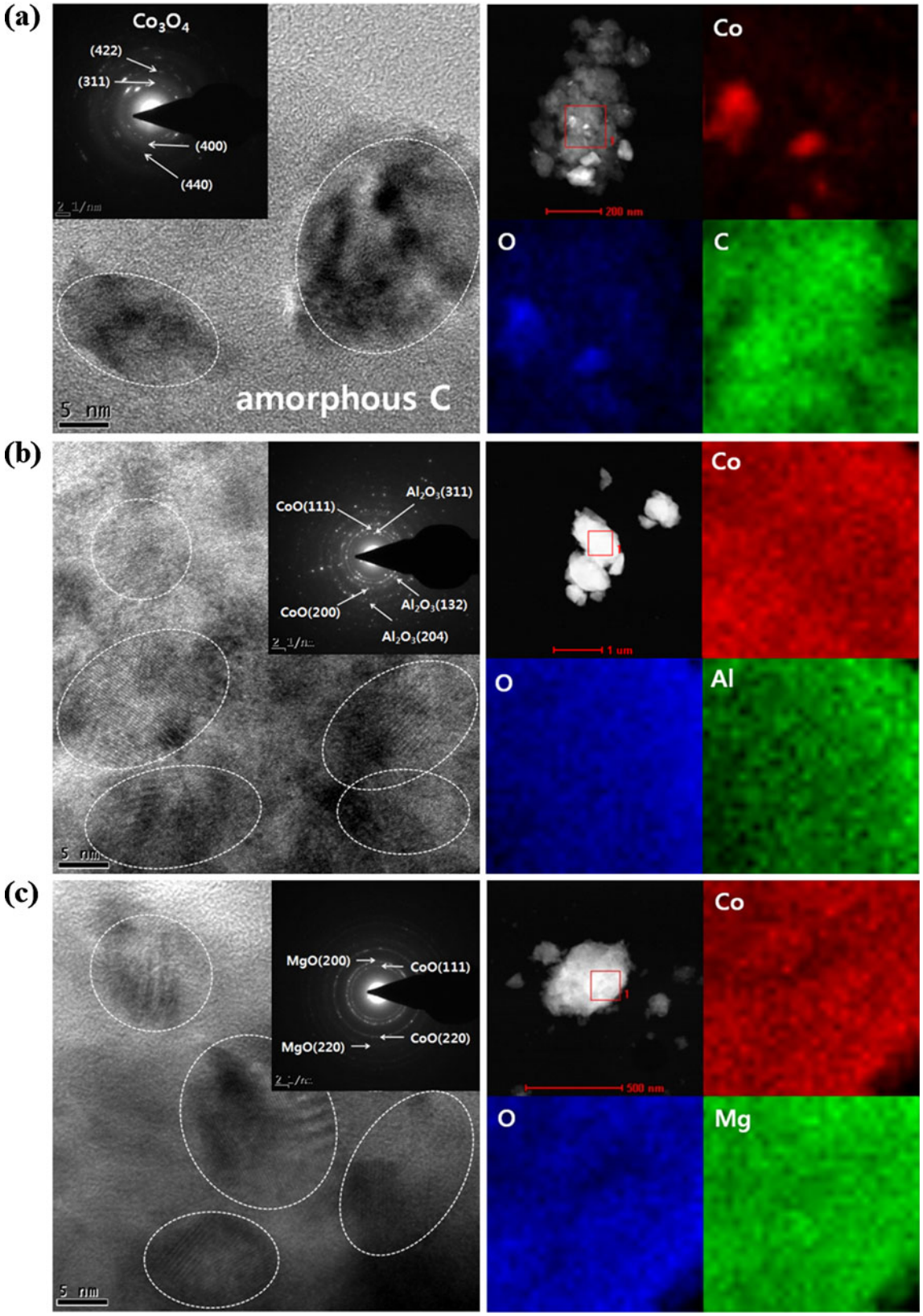

Fig. 3 HRTEM images with corresponding SAD patterns and EDS mapping images: **a** Co_3O_4/C, **b** CoO/Al_2O_3, and **c** CoO/MgO nanocomposites

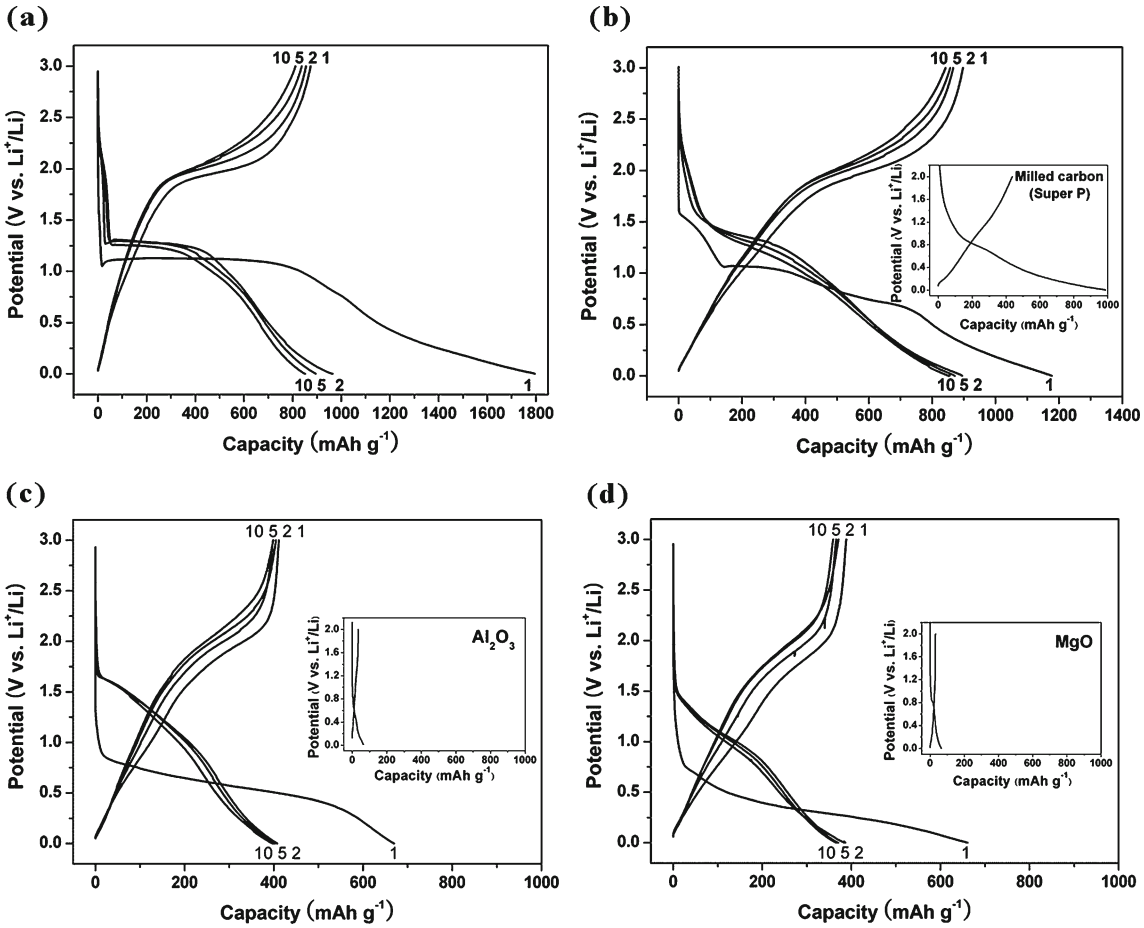

Fig. 4 Charge–discharge curves for the cobalt oxide-based nanocomposites: **a** Co_3O_4, **b** Co_3O_4/C (*inset*: charge–discharge curve for milled amorphous carbon), **c** CoO/Al_2O_3 (*inset*: charge–discharge curve for Al_2O_3), and **d** CoO/MgO (*inset*: charge–discharge curve for MgO) nanocomposite electrodes

(about 10–15 nm) within the Al_2O_3 matrix. The CoO/MgO nanocomposite also showed that well-dispersed CoO nanocrystallites with a size of approximately 10–15 nm were contained within the MgO matrix (Fig. 3c). The size of the nanocrystallite CoO in the CoO/Al_2O_3 and CoO/MgO nanocomposites agreed with that determined from the XRD pattern.

Figure 4a–d shows the voltage profiles of the Co_3O_4, Co_3O_4/C, CoO/Al_2O_3, and CoO/MgO nanocomposite electrodes, respectively. In Fig. 4a, the pure Co_3O_4 electrode showed a very low initial Coulombic efficiency (about 49%) and poor capacity retention (about 67% after 30th cycle); hence, it cannot be used as an anode material for Li-ion batteries. The low initial Coulombic efficiency and poor capacity retention resulted mainly from the formation of partially irreversible Li_2O phases and large volume changes associated with the pulverization of the micron-sized active material. In Fig. 4b, the first discharge and charge capacities of the Co_3O_4/C nanocomposite electrode are 1,170 and 880 mAh g^{-1}, respectively. The Coulombic efficiency of the Co_3O_4/C nanocomposite electrode for the first cycle is approximately 76%. The significantly enhanced initial Coulombic efficiency of the Co_3O_4/C nanocomposite electrode indicated that the electrochemical reaction between the

Table 1 Electrochemical data for the various nanostructured cobalt oxide-based composite electrodes

Electrodes	First discharge capacity [mAh g^{-1}]	First charge capacity [mAh g^{-1}]	First Coulombic efficiency [%]	Capacity retention after 30th cycle [%]
Co_3O_4	1,795	872	49	67
Co_3O_4/C	1,170	884	76	93
CoO/Al_2O_3	670	413	62	90
CoO/MgO	661	389	59	95

Co_3O_4 nanocrystallites (within the amorphous carbon matrix) and Li was considerably enhanced, considering the irreversible capacity of ball-milled amorphous carbon (~100 mAh g^{-1}, inset of Fig. 4b) in the Co_3O_4/C nanocomposite. The good initial Coulombic efficiency of the Co_3O_4/C nanocomposite electrode was attributed to the enhancement of the electrical conductivity by the carbon matrix, and the enhanced reversibility of nanocrystalline Co_3O_4 uniformly embedded within the nanocomposite. Figure 4c and d shows the voltage profiles of the first, second, fifth, and tenth cycles for the CoO/Al_2O_3 and CoO/MgO nanocomposite electrodes, respectively. Although these nanocomposite electrodes showed an enhanced initial Coulombic efficiency of 62% and 59%, respectively, when compared to the Co_3O_4 electrode, these values are not better than that for the Co_3O_4/C nanocomposite electrode. This observation indicated that the carbon matrix, having better electrical conductivity, is better than a ceramic matrix for the good electrochemical reversibility of Li-ion battery electrodes. The first charge capacities of CoO/Al_2O_3 and CoO/MgO electrodes were relatively small (413 and 389 mAh g^{-1}, respectively), which were attributed to a Li_2O formation reaction involving CoO (theoretical capacity, 715 mAh g^{-1}) [4, 11, 17] and to the presence of inactive ceramic matrices, such as Al_2O_3 and MgO phases (insets Fig. 4c and d). On the basis of the above results, it could be concluded that the initial Coulombic efficiency of cobalt oxide-based nanocomposite electrodes was mainly related to the nanocrystallites of the active material and to the presence of high electrical conductivity paths between nanocrystallites. In Table 1, the first discharge and charge capacities, the initial Coulombic efficiency, and the capacity retention after 30 cycles are listed.

Although ex situ XRD analyses of the Co_3O_4/C and the CoO/Al_2O_3 nanocomposite electrodes were performed at the half-lithiated (0.9 V, Co_3O_4/C; 0.7 V, CoO/Al_2O_3), fully lithiated (0 V), and fully delithiated (3.0 V) potentials in order to observe the structural changes occurring in the active materials (Co_3O_4 and CoO) as a result of the cycling, no structural changes were observed during the cycling (Fig. 5). Amorphization of XRD peaks of Co_3O_4/C and the CoO/Al_2O_3 nanocomposite electrodes demonstrates that active nanocrystalline cobalt oxides are well dispersed into smaller sized nanocrystallites during Li insertion/extraction.

Figure 6a and b shows differential capacity plots (DCP) of the first and second cycles for the Co_3O_4/C (with Co_3O_4)

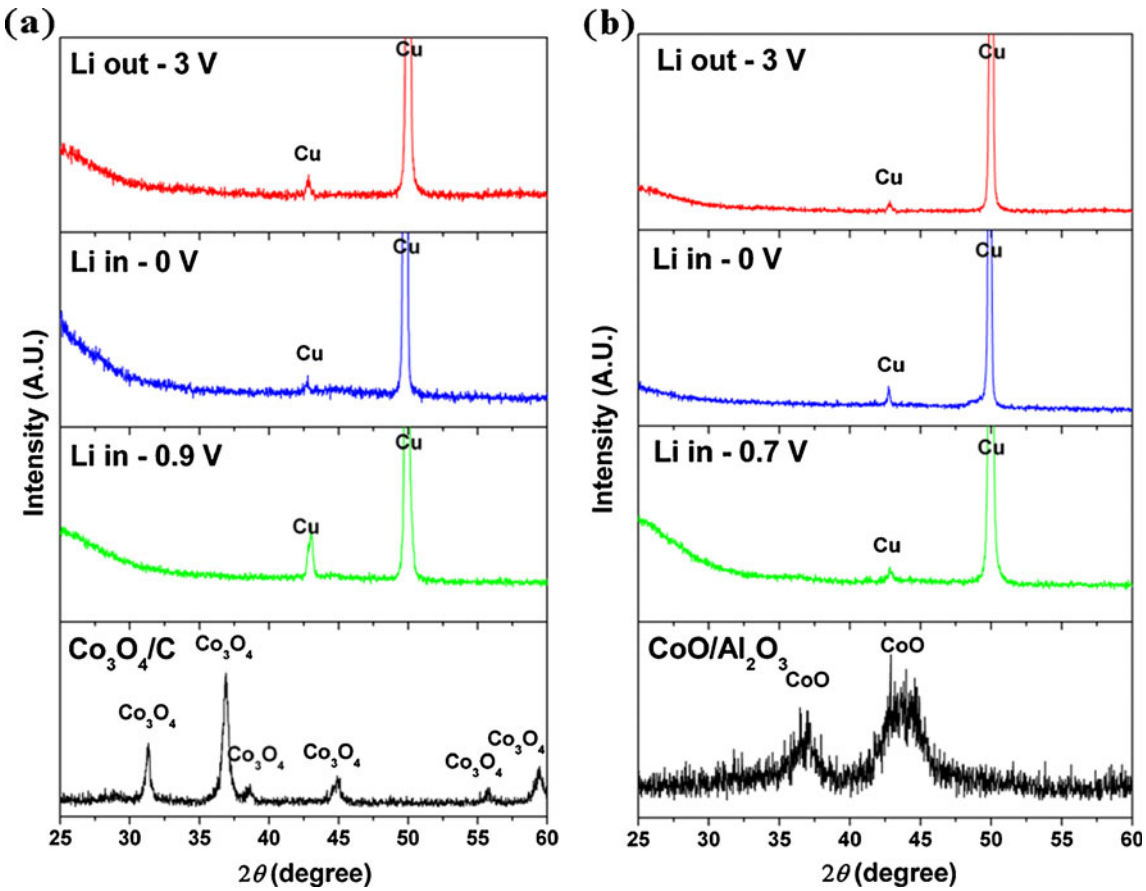

Fig. 5 Ex situ XRD results: **a** Co_3O_4/C and **b** CoO/Al_2O_3 nanocomposite electrodes

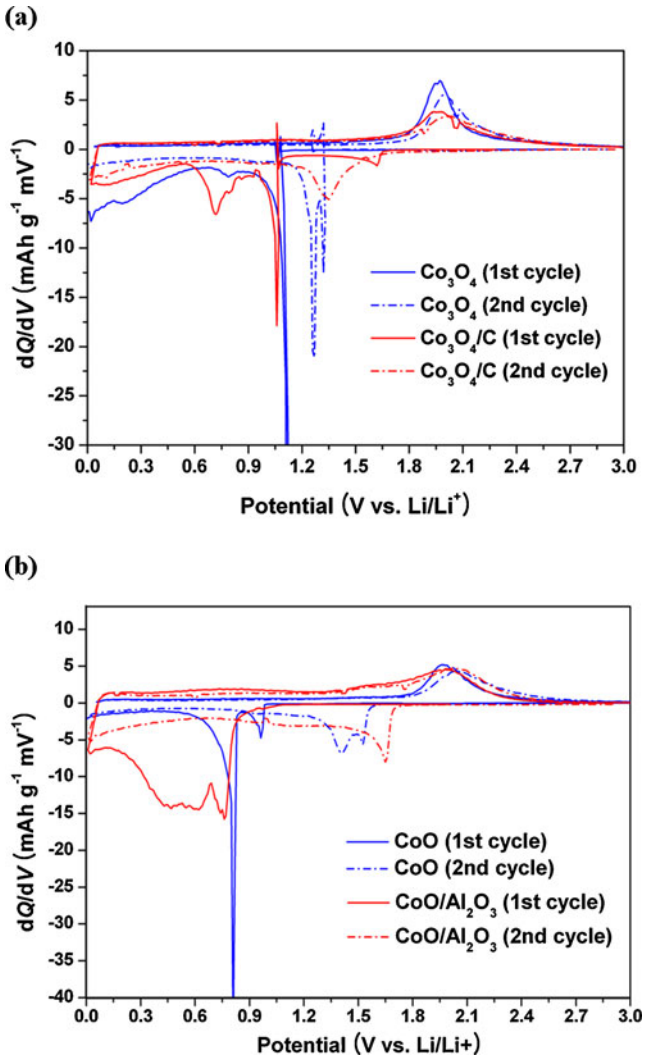

Fig. 6 Differential capacity plots for the cobalt oxide-based nanocomposites: **a** Co_3O_4/C and **b** CoO/Al_2O_3 nanocomposite electrodes

and CoO/Al_2O_3 (with CoO) nanocomposite electrodes, respectively. The DCP peaks of pristine electrodes for cobalt oxides (Co_3O_4 and CoO) are almost similar with those of their corresponding nanocomposite (Co_3O_4/C and CoO/Al_2O_3) electrodes. DCP peak broadening of Co_3O_4/C and CoO/Al_2O_3 nanocomposite electrodes was observed, which is related with reduced crystallinity of active cobalt oxides within nanocomposites. The DCP results were in agreement with those presented in other reports [4, 9, 11, 15]. Therefore, the reaction mechanisms of Co_3O_4 and CoO could be summarized as following electrochemical conversion reactions:

$$Co_3O_4 + 8Li^+ + 8e^- \leftrightarrows 4Li_2O + 3Co \quad (3)$$

$$CoO + 2Li^+ + 2e^- \leftrightarrows Li_2O + Co \quad (4)$$

The cycle performances of the Co_3O_4, Co_3O_4/C, CoO/Al_2O_3, and CoO/MgO nanocomposite electrodes at a current of 100 mA g^{-1} were compared. As shown in Fig. 7, the cycle performances of the all nanocomposite electrodes were quite good compared with that of Co_3O_4 electrode. The capacity retention of all the nanocomposite electrodes was above 90% after 30 cycles better than that of the pure Co_3O_4 electrode (67% after 30 cycles; Table 1). The Co_3O_4/C nanocomposite electrode showed good electrochemical characteristics, such as a very large first charge capacity of 884 mAh g^{-1}, high initial Coulombic efficiency of 76%, and high-capacity retention of 93%. Although the CoO/Al_2O_3 and CoO/MgO nanocomposite electrodes showed better electrochemical behaviors, such as enhanced initial Coulombic efficiency and higher-capacity retention, than those of the Co_3O_4 electrode, their first charge capacities were relatively small (413 and 389 mAh g^{-1}, respectively). The small charge capacities of the above electrodes were attributed to a Li_2O formation reaction involving CoO (theoretical capacity, 715 mAh g^{-1}) [4, 11, 17] and to the presence of inactive ceramic matrices, such as Al_2O_3 and MgO phases [24–27]. The good electrochemical properties of all nanocomposite electrodes were attributed to the following factors: the uniform distribution of active nanocrystallites in the matrix and the buffering effect of the various matrices, such as carbon and ceramics. Among the above matrices, the carbon matrix, having higher electrical conductivity [27–29], was better than the ceramic matrix because it facilitated better electrochemical reversibility of cobalt oxide-based electrodes.

Conclusions

Various nanostructured cobalt oxide-based composites, such as Co_3O_4/C, CoO/Al_2O_3, and CoO/MgO, were prepared by a simple HEMM in an attempt to enhance the electrochemical properties of Co_3O_4. When used as anode materials in

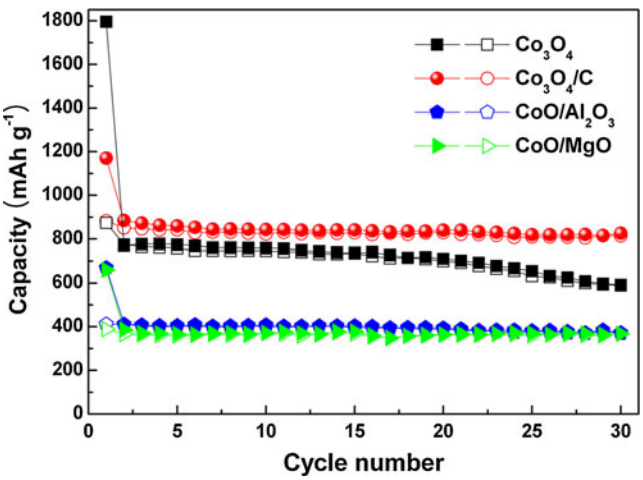

Fig. 7 Cycle performances of the Co_3O_4, Co_3O_4/C, CoO/Al_2O_3, and CoO/MgO nanocomposites (current rate, 100 mA g^{-1})

Li rechargeable batteries, all the nanocomposite electrodes showed enhanced electrochemical behaviors. The nanocomposite electrodes with a carbon matrix showed better electrochemical reversibility than other nanocomposite electrodes with ceramic matrices (Al_2O_3 and MgO). The large capacity, high initial Coulombic efficiency, and long cyclability of the Co_3O_4/C nanocomposite electrode were attributed to a nanostructure consisting of active nanocrystallites (Co_3O_4) within the conducting amorphous carbon matrix. Overall, the nanostructured Co_3O_4/C composite is a potential anode material for Li-ion batteries.

Acknowledgments Financial support by Korea Evaluation Institute of Industrial Technology grant funded by the Korean Government Ministry of Knowledge Economy (No. 10037148).

References

1. Huggins RA (1999) J Power Sources 81:13–19
2. Park CM, Kim JH, Kim H, Sohn HJ (2010) Chem Soc Rev 39:3115–3141
3. Winter M, Besenhard JO, Spahr M, Novak P (1998) Adv Mater 10:725–763
4. Poizot P, Laruelle S, Grugeon S, Dupont L, Tarascon JM (2000) Nature 407:496–499
5. Poizot P, Laruelle S, Grugeon S, Tarascon JM (2002) J Electrochem Soc 149:A1212–A1217
6. Larcher D, Sudant G, Leriche JB, Chabre Y, Tarascon JM (2002) J Electrochem Soc 149:A234–A241
7. Leroux F, Goward GR, Power WP, Nazar LF (1999) Electrochem Solid State Lett 1:255–257
8. Kim J, Cho J (2007) Electrochem Solid State Lett 10:A81–A84
9. Kang YM, Song MS, Kim JH, Kim HS, Park MS, Lee JY, Liu HK, Dou SX (2005) Electrochim Acta 50:3667–3673
10. Zhang P, Guo ZP, Huang Y, Jia D, Liu HK (2011) J Power Sources 196:6987–6991
11. Connor PA, Irvine JTS (2000) Ionics 6:428–433
12. Kang YM, Kim KT, Lee KY, Lee SJ, Jung JH, Lee JY (2003) J Electrochem Soc 150:A1538–A1543
13. Li B, Cao H, Shao J, Li G, Qu M, Yin G (2011) Inorg Chem 50:1628–1632
14. Xu R, Wang J, Li Q, Sun G, Wang E, Li S, Gu J, Ju M (2009) J Solid State Chem 182:3177–3182
15. Wu ZS, Ren W, Wen L, Gao L, Zhao J, Chen Z, Zhou G, Li F, Cheng HM (2010) ACS nano 4:3187–3194
16. Wang G, Liu J, Tang S, Li H, Cao D (2011) J Solid State Electrochem 15:2587–2592
17. Yao W, Chen J, Cheng H (2011) J Solid State Electrochem 15:183–188
18. Bruce PG, Scrosati B, Tarascon JM (2008) Angew Chem Int Ed 47:2930–2946
19. Chan CK, Peng H, Liu G, Mcilwrath K, Zhang XF, Huggins RA, Cui Y (2008) Nat Nanotechnol 3:31–35
20. Park CM, Sohn HJ (2010) Adv Mater 22:47–52
21. Park CM, Jeon KJ (2011) Chem Comm 47:2122–2124
22. Gleiter H (1989) Prog Mater Sci 33:223–315
23. Suryanarayana C (2001) Prog Mater Sci 46:1–184
24. Park CM, Sohn HJ (2008) Chem Mater 20:3169–3173
25. Park CM, Yoon S, Lee SI, Sohn HJ (2009) J Power Sources 186:206–210
26. Wang Y, Zhang YF, Liu HR, Yu SJ, Qin QZ (2003) Electrochim Acta 48:4253–4259
27. Yoon S, Manthiram A (2009) Chem Mater 21:3898–3904
28. Flahaut E, Peigney A, Laurent Ch, Marliere Ch, Chastel F, Rousset A (2000) Acta Mater 48:3803–3812
29. Chen Y, Kernohan RH, Boldu JL, Abraham MM (1980) Solid State Commun 33:441–443